Prediction of Low-Velocity Impact Damage in Thin Circular Laminates

K. N. Shivakumar*
Old Dominion University, Norfolk, Virginia
and
W. Elber† and W. Illg‡
NASA Langley Research Center, Hampton, Virginia

Clamped circular composite plates were analyzed for static equivalent impact loads. Three plate sizes—25.4, 38.1, and 50.8 mm radii—made of quasi-isotropic graphite/epoxy laminate were analyzed. The analysis was based on the minimum total potential energy method and used the von Kármán strain-displacement equations. A step-by-step incremental transverse displacement procedure was used to calculate plate load and ply stresses. The ply failure region and modes (splitting and fiber break) were calculated using the Tsai-Wu and the maximum stress criteria, respectively. Reduced moduli were then used in the failed region in subsequent increments of analyses. The analysis predicted that the failure would initiate as splitting in the bottom-most ply and then progress to other plies. Larger radii plates had a lower splitting threshold (load or energy) and a higher first-fiber failure threshold. The size and shape of the ply damage regions were different for different plies. The bottom ply damage was the largest and elongated in its ply-fiber direction. Calculated splitting damage for a 25.4 mm radius plate agreed with reported test data.

Nomenclature

a	= plate radius, m
a_c	= contact radius, m
$A_{11},A_{12},A_{22},A_{23}$, B_1,B_2,D_1,D_2	= constants defined in Appendix
C_1,C_2	= radial displacement constants
C_1',C_2'	= constants; $C_1'=C_1 w_0^2/a^3$, $C_2'=C_2 w_0^2/a^4$
E	= modulus, Pa
$E_{rr},E_{\theta\theta},E_{r\theta}$	= lamina stiffness in r-θ system, N/m^2
$F's$	= lamina strength parameters, defined in Appendix
G	= shear modulus, Pa
h	= plate thickness, m
N_L	= number of layers
N_R,N_θ	= number of divisions in radial and circumferential directions, respectively
P	= plate load, N
$q(r)$	= load intensity, N/m^2
r,θ,z	= polar coordinates, m, deg, m, respectively
$\bar{r}$	= average radius of a typical element ($\bar{r}=r_j$, see Appendix)
S	= lamina shear strength, Pa
U	= strain energy, N·m (J)
u	= radial deflection, m
V	= potential energy due to loading, N·m
w	= transverse deflection, m
w_0	= central, transverse deflection, m
X,X'	= lamina tensile and compressive strengths in fiber direction, Pa
Y,Y'	= lamina tensile and compressive strengths perpendicular to fiber direction, Pa
x,y,z	= Cartesian coordinates, m
α	= ply fiber angle
β	= $2\pi-\alpha-\theta$
Δ_{jk}	= area of a typical element (see Appendix)
ϵ	= in-plane strain
$\bar{\theta}$	= tangential coordinate at the center of a typical element
Π	= total potential energy, N·m
ν	= Poisson ratio
σ	= in-plane stress, N/m^2

Subscripts

i,j,k	= dummy subscripts, range of 1-N_L, 1-N_R, and 1-N_θ, respectively
ℓ	= longitudinal (fiber) direction
t	= transverse (fiber) direction
r	= radial direction
θ	= circumferential direction

Presented as Paper 83-0997 at the AIAA/ASME/ASCE/AHS 24th Structures, Structural Dynamics and Materials Conference, Lake Tahoe, Nev., May 2-4, 1983; received June 2, 1983; revision submitted June 6, 1984. This paper is declared a work of the U.S. Government and therefore is in the public domain.

*Research Associate Professor. Member AIAA.
†Assistant Head, Fatigue and Fracture Branch.
‡Senior Scientist, Fatigue and Fracture Branch.

Introduction

GRAPHITE fiber composites have a high strength-to-weight ratio, but are much more brittle than most metals. Therefore, they are easily damaged by impacts, especially those perpendicular to the laminate plane. Even low-velocity impacts from dropped tools can cause substantial damage. Often, the residual strength can be significantly reduced by impacts that leave no visible damage.

The study of such impact problems can be divided into three distinct areas: deformation mechanics, damage mechanics, and residual strength degradation. A systematic study of these three areas, in that order, will help to provide a basis for both design guidelines and materials development. The present study uses previously validated impact deformation mechanics to address the second area, that is, damage mechanics.

Most low-velocity impact problems can be treated as quasistatic problems,[1-3] because the impact duration is much longer than the time required by the propagating waves to travel from the impact site to the supports or free edges. Furthermore, studies[3-5] have shown that the impact tests and equivalent static tests produce essentially the same damage in thin composite laminates. Therefore, the analysis presented

here will assume slow transverse (perpendicular to the laminate plane) loading.

Thin composite plates undergo large deflection when loaded transversely, as shown in static load deflection tests by Bostaph and Elber[4] and impact tests by Elber.[5] The large displacements introduce geometric nonlinearity in the stress analysis of thin plates.

The objectives of the present study were to develop a stress analysis including the effects of geometric nonlinearity and then to calculate the displacements that cause initiation and progression of damage in circular composite plates. Damage modes were analytically limited to ply splits and fiber breaks. The laminate layup was assumed to be quasi-isotropic, although quasi-isotropic laminates are flexurally anisotropic. Therefore, for simplicity, plate deformations were assumed to be axisymmetric under the central plate loading.

For the purpose of numerical analysis, the plate was divided radially, circumferentially, and axially (thickness direction) into a number of parts. Using the von Kármán strain-displacement equation, the strain energies of individual elements were calculated and then summed over all elements to obtain the total strain energy of the deformed plate. Next, the sum of strain energy and the potential energy due to loading was minimized with respect to displacement constants. The resulting equations were solved numerically using an incremental transverse deflection procedure. Ply stresses in each element were calculated and the plate was examined for failure using the Tsai-Wu and maximum stress criteria. The analysis was continued for additional increments of displacements using reduced moduli in failed elements. Load-deflection curves and damage plots are presented for three plate sizes. Damage sizes are compared with test results from Ref. 5.

Analysis

Plate Configuration and Loading

Figure 1 shows the plan view and the cross-sectional view of a clamped circular plate of thickness h and radius a, loaded by a sphere at its center. The plate was assumed to be made of T300/5208 (Thornel 300/Normco 5208)[§] graphite/epoxy with a quasi-isotropic layup $[45/0/-45/90]_s$. Because the plate is circular, this layup is equivalent to $[0/-45/90/45]_s$, $[-45/90/45/0]_s$, etc. The Cartesian and polar coordinate system is shown in Fig. 1. The w and u are the plate middle surface displacements in the transverse and radial directions, respectively. The fiber orientation in any layer was represented by an angle α and measured from the x axis as shown in the figure. The plate loads were applied by a 12.7 mm radius steel sphere.

For the purpose of numerical analysis, the plate was divided into an axisymmetric arrangement of elements as shown schematically in Fig. 2. The actual model had a much more dense array of elements, defined by dividing the plate radius into 50 intervals and the plate circumference into 108 intervals. In the thickness direction, each ply was represented by one element. A typical element (see shaded region) was defined by the radial coordinates r_j and r_{j+1}, the tangential coordinates θ_k and θ_{k+1}, and axial or thickness coordinates z_i and z_{i+1}.

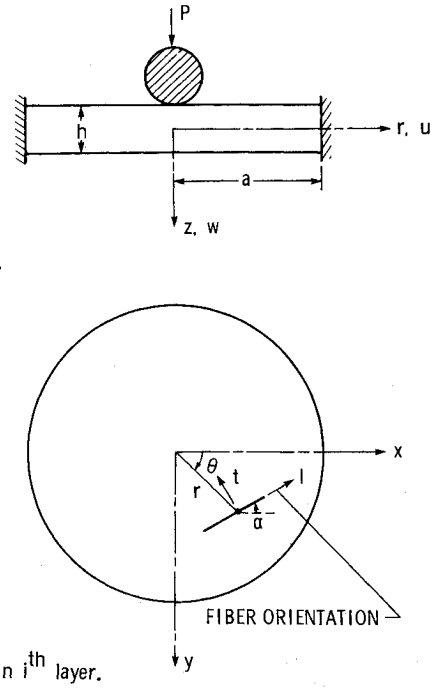

Fig. 1 Clamped circular plate with coordinate system.

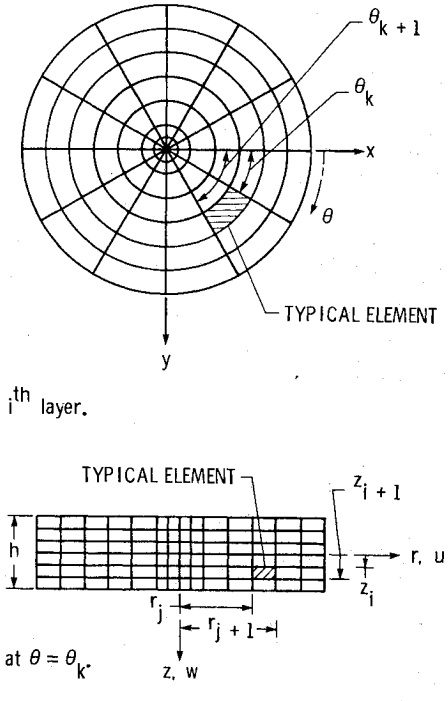

Fig. 2 Schematic idealization of a laminated plate.

Analytical Approach

The analysis was based on the minimization of total potential energy. A set of displacement functions was selected that satisfied the following three assumptions: 1) the circular, quasi-isotropic plate deforms axisymmetrically under an axisymmetric load; 2) the deformed shape of the plate for large deflections is the same as that for small deflections[6]; and 3) because the plate is thin ($a/h > 10$), the transverse shear deformation is negligible. The axisymmetric assumption is not exact, because the quasi-isotropic laminate is, in general, flexurally anisotropic. However, the flexural anisotropy is small and becomes insignificant for a large number of layers.[7] A general description of the approach follows.

An incremental transverse displacement procedure was used to calculate the constants in the radial displacement function. Ply stresses (in the ℓ-t coordinate system) were then calculated from the complete displacement functions. The Tsai-Wu criterion was used to determine when the stresses were high enough to cause failure in each element. Once the

§Use of trade name or manufacturers does not constitute an official endorsement, either expressed or implied, by the National Aeronautics and Space Administration.

Tsai-Wu criterion indicated a failure, the mode of failure (splitting or fiber failure) was taken as that mode most nearly satisfying the maximum stress criteria. Splitting failures could be caused by transverse tension stress or by in-plane shear stress. The failure of an element by splitting or by fiber failure was simulated by reducing the appropriate moduli to zero. The transverse displacement was then incremented and the analysis was repeated. Because the process of reducing in-plane moduli increases flexural anisotropy, the present analysis was restricted to mildly damaged plates.

Energy Formulation

The midplane transverse displacement w and radial (in-plane) displacement u of a centrally loaded plate were taken from Ref. 6,

$$w = w_0\left[1-\left(\frac{r}{a}\right)^2+2\left(\frac{r}{a}\right)^2 \ell n\left(\frac{r}{a}\right)\right] \tag{1}$$

and

$$u = r(a-r)\,(C_1'+C_2' r) \tag{2a}$$

where w_0 is the central displacement of the plate, and C_1 and C_2 constants that were evaluated by minimizing the total potential energy of the deformed plate. The above two displacement functions satisfy all of the kinematic boundary conditions of the plate. At $r=0$, $u=\mathrm{d}w/\mathrm{d}r=0$, and at $r=a$, $u=w=\mathrm{d}w/\mathrm{d}r=0$. Furthermore, it was deduced from Ref. 6 that

$$C_1' = C_1 w_0^2/a^3 \quad \text{and} \quad C_2' = C_2 w_0^2/a^4$$

for small increments of w_0. Consequently, C_1 and C_2 were the independent constants to be evaluated. Equation (2a) was rewritten as

$$u = \frac{w_0^2}{a^3} r(a-r)\left(C_1+C_2\frac{r}{a}\right) \tag{2b}$$

Strain displacement relations for large deflections of the plate were written using von Kármán equations[8] as

$$\epsilon_r = \frac{\mathrm{d}u}{\mathrm{d}r}+\frac{1}{2}\left[\left(\frac{\mathrm{d}u}{\mathrm{d}r}\right)^2+\left(\frac{\mathrm{d}w}{\mathrm{d}r}\right)^2\right]-z\frac{\mathrm{d}^2 w}{\mathrm{d}r^2}$$

$$\epsilon_\theta = \frac{u}{r}-\frac{z}{r}\frac{\mathrm{d}w}{\mathrm{d}r}, \qquad \epsilon_{r\theta}=0 \tag{3}$$

where ϵ_r, ϵ_θ, and $\epsilon_{r\theta}$ are the radial, tangential, and shear strains, respectively. A second-order u-displacement term was included in Eqs. (3) because of expected very large displacements.[6]

The strain energy due to plate deformation was expressed as

$$U = \tfrac{1}{2}\int \sigma\epsilon\,\mathrm{d}v$$

where σ and ϵ are components of in-plane stresses and strains, respectively. Substituting for stress using standard stress-strain relations for orthotropic composite lamina[7] produced the strain energy equation

$$U = \frac{1}{2}\int_0^{2\pi}\int_0^{a}\int_{-h/2}^{h/2}(E_{rr}\epsilon_r^2+E_{\theta\theta}\epsilon_\theta^2+2E_{r\theta}\epsilon_r\epsilon_\theta)\,r\,\mathrm{d}z\,\mathrm{d}r\,\mathrm{d}\theta \tag{4}$$

The elastic stiffness parameters E_{rr}, $E_{\theta\theta}$, and $E_{r\theta}$ are defined in the Appendix. Integration of Eq. (4) was not practical due to the irregular damage shape. Hence, the summation approach was used. The total strain energy of the plate was computed as the sum of element strain energies for the plate model in Fig. 2. The strain energy of each element was expressed as the product of strain energy density at the element center and its volume. Therefore,

$$U = \frac{1}{2}\sum_{k=1}^{N_\theta}\sum_{j=1}^{N_R}\int_{-h/2}^{h/2}(E_{rr}\epsilon_r^2+E_{\theta\theta}\epsilon_\theta^2 +2E_{r\theta}\epsilon_r\epsilon_\theta)\,\mathrm{d}z\left(\frac{r_{j+1}^2-r_j^2}{2}\right)(\theta_{k+1}-\theta_k) \tag{5}$$

The N_R and N_θ are the number of divisions in the radial and circumferential directions, respectively (see Fig. 2) of the plate. For sufficently large values of N_R and N_θ, the summation equation (5) becomes equal to the integration equation (4). A complete strain energy expression can be obtained following the usual algebra, using Eqs. (1-3) and (5). Since the resulting expression is very lengthy, it is not presented here.

Figure 3 shows a typical load distribution $q(r)$ due to impact by a stiff sphere. The $q(r)$ is elliptic and is given in Ref. 3 as

$$q(r) = \frac{3P}{2\pi a_c^2}\left[1-\left(\frac{r}{a_c}\right)^2\right]^{1/2} \tag{6}$$

where P is the impact load and a_c the radius of contact between the sphere and the plate. The value of a_c can be calculated from Eq. (14) in Ref. 3 using the properties of the impactor and plate and the impact load.

The potential energy due to loading is

$$V = -\int_0^{a_c}\int_0^{2\pi} q(r)\,w\,r\,\mathrm{d}r\,\mathrm{d}\theta$$

Substituting for w from Eq. (1) and integrating, the expression for V becomes

$$V = -Pw_0\left[1-0.67515\left(\frac{a_c}{a}\right)^2+0.8\left(\frac{a_c}{a}\right)^2 \ell n\left(\frac{a_c}{a}\right)\right] \tag{7}$$

For very small values of a_c, Eq. (7) reduces to a point loading case, i.e., $V=-Pw_0$.

The total potential energy Π of the deformed plate is

$$\Pi = U+V \tag{8}$$

By substituting Eqs. (5) and (8), Π can be expressed as a function of the three unknown displacement constants, C_1, C_2, and w_0. Minimization of the total potential energy Π with respect to these three constants produced the following three equations:

$$A_{11}C_1+A_{12}C_2 = -B_1-D_1 \tag{9}$$

$$A_{12}C_1+A_{22}C_2 = -B_2-D_2 \tag{10}$$

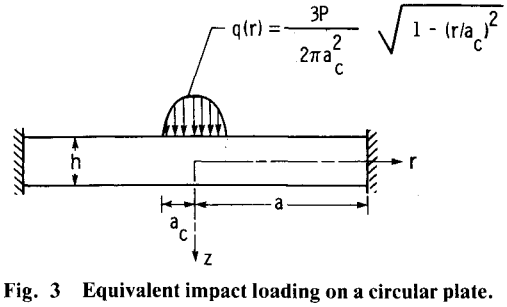

Fig. 3 Equivalent impact loading on a circular plate.

$$A_{33}(C_1,C_2,w_0)=P\left[1-0.67515\left(\frac{a_c}{a}\right)^2+0.8\left(\frac{a_c}{a}\right)^2\ell_n\left(\frac{a_c}{a}\right)^2\right] \quad (11)$$

The expressions for A_{11}, A_{12}, A_{22}, A_{33}, B_1, B_2, D_1, and D_2 are given in the Appendix. The solution of Eqs. (9-11) was not straightforward because of complex algebra [introduced due to the term $(du/dr)^2$ in Eqs. (3)] and the irregular damage shape developed during the loading. Hence, an iterative technique along with an incremental transverse deflection procedure was used. Furthermore, calculation of the load P requires the prior knowledge of the contact radius a_c; hence, the following procedure was employed. First, a point load was calculated for $a_c=0$ by solving Eqs. (9-11) iteratively. This value of the load and the properties of the sphere and laminate were used in Eq. (14) of Ref. 3 to calculate a_c. Finally, a corrected distributed load P was calculated corresponding to this value of a_c. Since the variation of a_c is very small from the first to subsequent iterations, only one iteration was used in this procedure. Details of the numerical procedure are presented in a subsequent section.

Failure Criteria

The Tsai-Wu quadratic failure criterion[9] was used to calculate damage regions and the maximum stress criteria[7] was used to identify the failure modes. First, normal and shear stresses in the ℓ-t coordinate system (see Fig. 1b) were calculated at the center of each element. Then the presence of element failure was determined using the Tsai-Wu criterion [Eq. (A6)]. Finally, the failed elements were re-examined using maximum stress criteria [Eq. (A8)] to determine whether the failure was splitting or fiber breakage. Splitting damage was due to either transverse tensile stress or in-plane shear stress, whereas fiber failure was due to longitudinal stress in the lamina. Figure 4 shows a schematic of a typical damage region. The damage was typically elongated in the fiber direction, with length ℓ_d and width w_d. Elements that failed by splitting were considered to have lost their transverse modulus E_t and their shear modulus $G_{\ell t}$. Hence, the reduced moduli ($E_t=G_{\ell t}=0$) were used in these failed elements in subsequent steps of the analysis.

Fiber failure was generally the last stage of element failure and causes the complete loss of stiffness. Fiber failure was calculated by comparing the stress in the fiber direction with the longitudinal lamina strength. Within the fiber failure region, the longitudinal modulus E_ℓ was also set equal to zero. The width of the fiber failure region is indicated by w_f in Fig. 4. For convenience, the region of complete failure ($E_\ell=E_t=G_{\ell t}=0$) is represented by the shaded rectangle. Therefore, all the moduli of all the elements lying within the shaded region were reduced to zero in the subsequent steps of the analysis. Equations used in the failure criteria are given in the Appendix.

Table 1 Elastic properties of plate and impactor

Material	Modulus, GPa E_ℓ	$E_{\ell t}$	$G_{\ell t}$	Poisson ratio $\nu_{\ell t}$
Gr/Ep lamina[a]	131.0	13.0	6.4	0.34
Gr/Ep laminate[b]	53.3	53.3	20.7	0.31
Steel ball	206.8	206.8	79.5	0.30

[a]Subscripts ℓ and t correspond to longitudinal and transverse directions of fibers (see Fig. 1b). [b]Laminate subscripts ℓ and t correspond to r and θ directions. $E_{zz}=14.5$ GPa, $G_{rz}=5.6$ GPa, and $\nu_{rz}=0.28$. Layup: $[45/0/-45/90]_s$.

Table 2 Lamina strengths, MPa

Longitudinal X	X'	Transverse Y	Y'	Shear S
1500	−1500	40	−246	68

Numerical Procedure

As previously mentioned, numerical results in the present analysis were obtained using an incremental transverse deflection procedure (Fig. 5). Starting with a value of w_0, the constants C_1 and C_2 and then the load P were calculated using the principle of minimum total potential energy. Then, failure regions were calculated on a ply-by-ply basis [Eqs. (9-11)]. After the appropriate elastic moduli in the failed regions were reduced, the analysis was repeated for the next incremental value of w_0. Relevant elastic properties and strength properties are given in Tables 1 and 2.

The step-by-step procedure is

1) Select initial and incremental values of w_0.
2) Increment w_0.
3) Calculate C_1 and C_2 from Eqs. (9) and (10), respectively.
4) Calculate load P from Eq. (11).
5) Check for failure using Eqs. (A6) and (A8).
6) If there is no failure, repeat steps 2-5 until failure develops.
7) Calculate the region of the splitting failure (see Fig. 4).
8) Calculate the width of the fiber failure region.
9) Reduce E_t and $G_{\ell t}$ to zero in the splitting damage region.
10) Reduce E_ℓ, E_t, and $G_{\ell t}$ to zero in the region of both splitting and fiber damage.
11) Repeat steps 3-10.

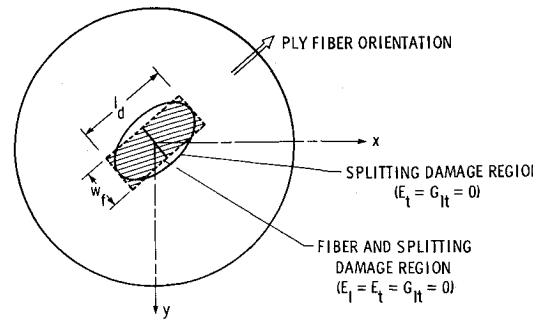

Fig. 4 Schematic of an *i*th ply damage.

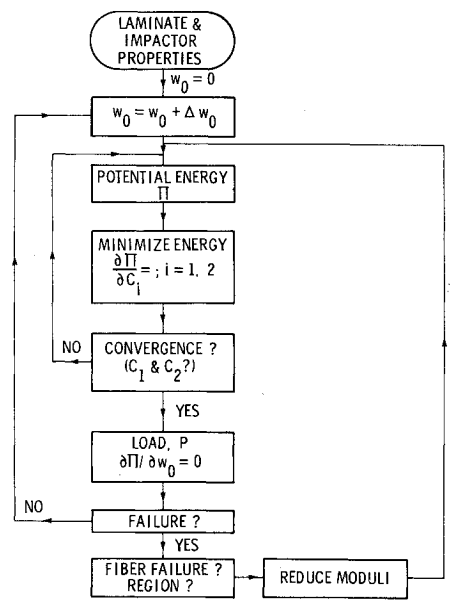

Fig. 5 Flow diagram of the numerical procedure.

Steps 2-11 were repeated until a preselected value of damage size, w_0, or load level was reached.

Results and Discussion

As a check on the present analysis, the case of an isotropic, circular plate with a point load was analyzed using several mesh sizes. The previously described mesh (50 radial and 108 circumferential divisions) produced displacements and stresses that agreed closely with the exact solution from Ref. 7. As a result, this grid size was used for all cases reported in this paper. Calculated load vs central deflection curves and damage plots for composite laminates are presented in this section. Calculated laminate damage lengths and fiber damage widths were compared with the Ref. 5 test results.

Figure 6 shows load P vs deflection w_0 for a 25.4 mm radius plate. Numbers beside the curves indicate ply numbers wherein the damage initiated. The superscript ff denotes fiber failure. At $w_0 = 0.29$ mm ($P = 0.14$ kN) the first failure, splitting, occurred in ply 8 (the bottom-most ply). Since the damage was small, the calculated loads before and after the failure were almost identical. At higher values of w_0, additional splitting damage developed in plies 7 and 6. At $w_0 = 1.04$ mm, splitting failure initiated in ply 5 and the first fiber failure occurred in ply 8. The load abruptly dropped from 0.73 to 0.68 kN. With a further increase in w_0, the damaged regions increased in size and fiber failures occurred in plies 1 (compressive failure), 7, and 6. The analysis was stopped at about $w_0 = 2.08$ mm because excessive fiber failures began to invalidate the axisymmetric deformation assumption.

Figure 7 shows the calculated ply damage at $w_0 = 0.94$ mm ($P = 0.61$ kN). At this displacement level, plies 6, 7, and 8 had developed splitting damage. The damage region was different in each ply and was elongated in the fiber direction. Such differences in the size and shape of the damages between any two adjacent plies would contribute to the separation of the plies (delamination) by introducing interply stresses. Furthermore, the damage region was largest in ply 8. In an ultrasonic C-scan of the damaged specimen, the damage in ply 8 would mask that in the other plies. To illustrate this masking effect, the individual ply damages are superimposed and are presented in Fig. 8 for a range of w_0 values. The load-deflection curve in Fig. 8 is the lower envelope of the curve in Fig. 6.

Figure 9 shows a comparison of the load-deflection curves for three plate sizes. As expected, the initial slopes are different. However, at large values of w_0, all three curves tend to have a similar steep slope due to membrane stiffening. The lower dashed curve is the splitting damage threshold and the upper dashed curve is the fiber damage threshold. The negative slope of the splitting threshold curve indicates that larger plates have lower threshold loads than the small plates. In contrast, the larger plates have a higher fiber damage threshold than the small plates. However, the above conclusion cannot be generalized because, at higher load levels, the penetration mechanism may become dominant[4,10] and the present analysis does not address such behavior.

Figure 9 also shows a comparison of the damage regions calculated for the three plate sizes at approximately the same load level. The damage is smallest for the 25.4 mm plate and largest for the 50.8 mm plate. Therefore, one can conclude that for a given load level and plate thickness, larger plates would be expected to develop larger damage regions.

Figure 10 shows a comparison of calculated damage length ℓ_d (see Fig. 4) with test results from Ref. 5 for a 25.4 mm plate. The symbols represent the static and impact test results and the solid curve represents the results from this analysis for the ply with largest damage (ply 8). This figure shows that the present analysis agrees well with the static test results, but overpredicts damage length compared to the impact test results.

Figure 11 shows fiber damage width w_f plotted against ply number for the 8-ply laminate. Again, the symbols represent test data from Ref. 5 and the solid curve corresponds to the present analysis. Comparison of two sets of results shows that the analysis predicts more fiber damage in ply 8 than that measured in the tests. This discrepancy may be explained by the unaccounted splitting-induced delamination freedom of ply 8, which reduces its fiber strains, in the analysis. Otherwise, the representation of the ply-by-ply damage is generally satisfactory.

Figure 12 shows the total fiber damage width (sum of the fiber failure widths for all plies) plotted for a range of impact

PLY NUMBER	PLY ANGLE (α)	DAMAGE
1	45°	NONE, 10 mm
2	0°	NONE
3	-45°	NONE
4	90°	NONE
5	90°	NONE
6	-45°	
7	0°	
8	45°	

Fig. 7 Predicted ply damage at $w_0 = 0.94$ mm ($P = 0.61$ kN) ($a = 25.4$ mm, $h = 1.04$ mm).

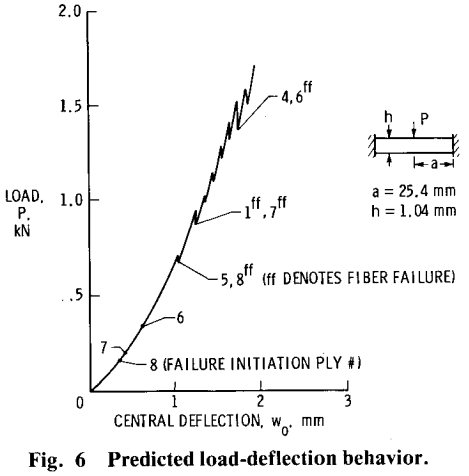

Fig. 6 Predicted load-deflection behavior.

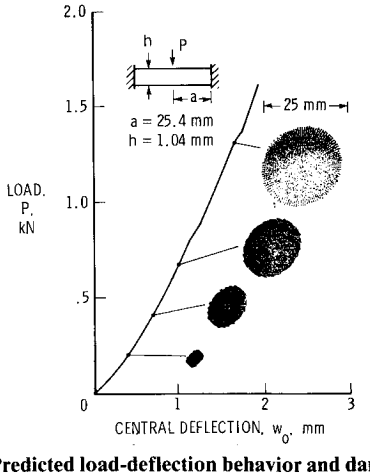

Fig. 8 Predicted load-deflection behavior and damage regions.

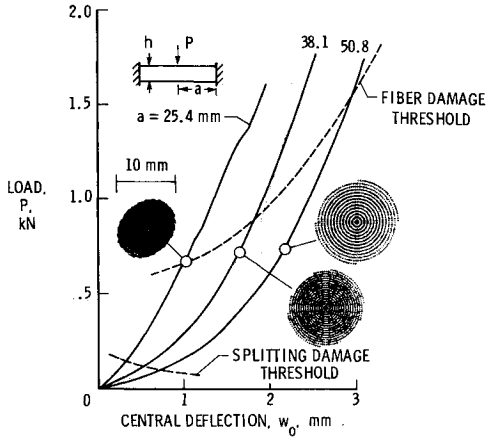

Fig. 9 Predicted load-deflection behavior for three plate radii.

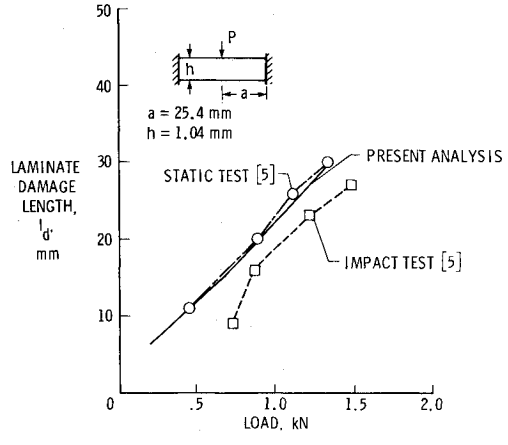

Fig. 10 Comparison of predicted and measured damage lengths of an 8-ply laminate.

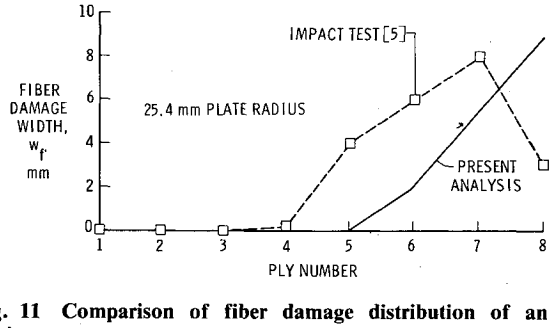

Fig. 11 Comparison of fiber damage distribution of an 8-ply laminate.

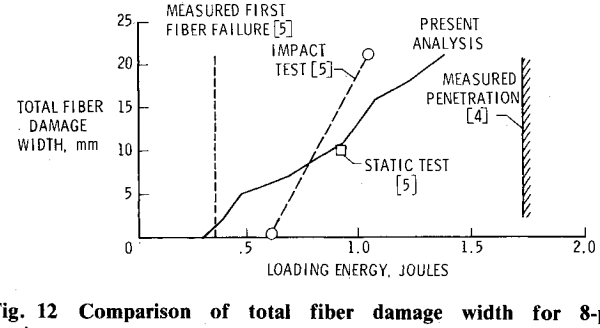

Fig. 12 Comparison of total fiber damage width for 8-ply laminates.

loading energies. The loading energy in this figure corresponds to the area under the load-deflection curve (for example, see Fig. 6). Figure 12 has both test data and calculated results for a 25.4 mm radius plate as well as calculated curves for 38.1 and 50.8 mm radii plates. The dashed vertical line on the left represents the threshold fiber failure energy measured for a 25.4 mm radius plate.[5] The solid vertical line at 1.72 J represents the measured penetration energy for the 8-ply laminate with a 12.7 mm radius sphere.[4]

Comparison of the calculated and test results for the 25.4 mm radius plate shows that the one static test result lies close to the analysis curve, but the impact test curve crosses the analysis curve. However, the calculated first fiber failure energy was very close to the test value. Figure 12 also shows that the fiber failure threshold energy should increase with the plate size. The smaller plates would develop extensive fiber failure damage before reaching the penetration threshold energy, whereas the larger plates would tend to fail by penetration. Thus, for a given plate thickness, impactor radius, and a limited a/h range ($a/h>10$), the smaller plates should fail due to high in-plane stresses, whereas the larger plates would fail by other modes such as penetration.

Conclusions

Clamped circular composite plates were analyzed for static equivalent impact loads. The plates consisted of T300/5208 graphite/epoxy in an 8-ply, quasi-isotropic layup and were analyzed for three sizes: 25.4, 38.1, and 50.8 mm radii. The analysis was based on the minimum total potential energy method and the von Kármán strain displacement equations. A step-by-step incremental transverse displacement procedure was used to calculate plate load and ply stresses. The ply failure region was calculated using the Tsai-Wu criterion. The corresponding failure modes (limited to splitting and fiber failure) were determined using the maximum stress criteria. Reduced elastic moduli were then used in the failed region in subsequent increments of analyses. This analysis led to the following conclusions:

1) The first failure mode was splitting and initiated first in the bottom-most ply.

2) The splitting failure thresholds were relatively low and tended to be lower for larger plates than for small plates.

3) The splitting damage region in each ply was elongated in its fiber direction; the bottom ply had the largest damage region.

4) Larger plates developed larger splitting damage regions than smaller plates subjected to the same transverse load.

5) The calculated damage region for the 25.4 mm radius plate agreed with limited static test results from the literature.

6) First fiber failure thresholds (load or energy) are higher for large plates than for small plates over a limited range of radius-to-thickness ratio ($a/h>10$).

Appendix

This Appendix presents the following supporting equations used in the present study: lamina stiffness expressions in r-θ coordinate system, definitions of constants used in Eqs. (9-11), and failure criteria equations.

Lamina Stiffness Expressions in r-θ Coordinate System

Expressions for E_{rr}, $E_{\theta\theta}$, and $E_{r\theta}$ were taken from Ref. 6, and were rewritten in terms of the angle $\beta=(2\pi-\theta-\alpha)$.

$$E_{rr}=E_{11}\cos^4\beta+2(E_{12}+2E_{66})\sin^2\beta\cos^2\beta+E_{22}\sin^4\beta$$

$$E_{\theta\theta}=E_{11}\sin^4\beta+2(E_{12}+2E_{66})\sin^2\beta\cos^2\beta+E_{22}\cos^4\beta$$

$$E_{r\theta}=(E_{11}+E_{22}-4E_{66})\sin^2\beta\cos^2\beta+E_{12}(\sin^4\beta+\cos^4\beta) \quad \text{(A1)}$$

where

$$E_{11}=\frac{E_\ell}{(1-\nu_{\ell t}\nu_{t\ell})},\qquad E_{22}=\frac{E_t}{(1-\nu_{\ell t}\nu_{t\ell})}$$

$$E_{12}=\frac{\nu_{\ell t}E_t}{(1-\nu_{\ell t}\nu_{t\ell})},\qquad E_{66}=G_{\ell t} \tag{A2}$$

where E_ℓ, E_t, $G_{\ell t}$, and $\nu_{\ell t}$ are the standard elastic properties for an orthotropic lamina. The subscripts ℓ and t represent the longitudinal and transverse directions with respect to the lamina fibers (see Fig. 1b).

Constants in Equations (9-11)

The constants used in Eqs. (9-11) are defined as follows:

$$A_{11}=\sum_{i=1}^{N_L}\sum_{j=1}^{N_R}\sum_{k=1}^{N_\theta}(z_{i+1}-z_i)A'_{11}\Delta_{jk}$$

$$A_{12}=\sum\sum\sum(z_{i+1}-z_i)A'_{12}\Delta_{jk}$$

$$A_{22}=\sum\sum\sum(z_{i+1}-z_i)A'_{22}\Delta_{jk}$$

$$B_1=\sum\sum\sum\left(\frac{z_{i+1}-z_i}{2}\right)B'_1\Delta_{jk}$$

$$B_2=\sum\sum\sum\left(\frac{z_{i+1}-z_i}{2}\right)B'_2\Delta_{jk}$$

$$D_1=\sum\sum\sum\left(\frac{z_{i+1}-z_i}{2}\right)D'_1\Delta_{jk}$$

$$D_2=\sum\sum\sum\left(\frac{z_{i+1}-z_i}{2}\right)D'_2\Delta_{jk}$$

$$A_{33}=\sum\sum\sum A'_{33}\Delta_{jk} \tag{A3}$$

where

$$A'_{11}=(a-2\bar r)^2E_{\bar r\bar r}+(a-\bar r)^2E_{\bar\theta\bar\theta}+2E_{\bar r\bar\theta}(a-\bar r)(a-2\bar r)$$
$$-\left(\frac{z_{i+1}+z_i}{2}\right)(a-2\bar r)^2\left(E_{\bar r\bar r}w''+\frac{E_{\bar r\bar\theta}}{\bar r}w'\right)$$

$$A'_{12}=\bar r(a-2\bar r)(2a-3\bar r)E_{\bar r\bar r}+\bar r(a-\bar r)(3a-5\bar r)E_{\bar r\bar\theta}$$
$$+\bar r(a-\bar r)^2E_{\bar\theta\bar\theta}-\left(\frac{z_{i+1}+z_i}{2}\right)(a-2\bar r)(2a-3\bar r)$$
$$\times(E_{\bar r\bar r}\bar rw''+E_{\bar r\bar\theta}w')$$

$$A'_{22}=\bar r^2(2a-3\bar r)^2E_{\bar r\bar r}+\bar r^2(a-\bar r)(2a-3\bar r)E_{\bar r\bar\theta}$$
$$+\bar r^2(a-\bar r)^2E_{\bar\theta\bar\theta}-\left(\frac{z_{i+1}+z_i}{2}\right)\bar r(2a-3\bar r)^2\ (E_{\bar r\bar r}\bar rw''+E_{\bar r\bar\theta}w')$$

$$B'_1=[(a-2\bar r)E_{\bar r\bar r}+(a-\bar r)E_{\bar r\bar\theta}](w')^2+(z_{i+1}+z_i)$$
$$\times\left\{E_{\bar r\bar r}(a-2\bar r)w''+E_{\bar\theta\bar\theta}\left(\frac{a}{\bar r}\right)w'+E_{\bar r\bar\theta}\left[(a-\bar r)w''+\left(\frac{a-2\bar r}{\bar r}\right)w'\right]\right\}$$

$$B'_2=[\bar r(2a-3\bar r)E_{\bar r\bar r}+\bar r(a-\bar r)E_{\bar r\bar\theta}](w')^2+(z_{i+1}+z_i)$$
$$\times\{E_{\bar r\bar r}(2a-3\bar r)\bar rw''+E_{\bar\theta\bar\theta}(a-\bar r)w'+E_{\bar r\bar\theta}[(a-\bar r)\bar rw''$$
$$+(2a-3\bar r)w']\}$$

$$D'_1=E_{\bar r\bar r}(a-2\bar r)u'[(u')^2+3u'+(w')^2]$$
$$+E_{\bar r\bar\theta}u'\left[(a-\bar r)u'+\frac{2u}{\bar r}(a-2\bar r)\right]$$

$$D'_2=E_{\bar r\bar r}(2a-3\bar r)\bar ru'[(u')^2+3u'+(w')^2]$$
$$+E_{\bar r\bar\theta}u'[\bar r(a-\bar r)+2u(2a-3\bar r)]$$

$$A'_{33}=\left(\frac{z_{i+1}-z_i}{2w_0}\right)\left\{E_{\bar r\bar r}[4(u')^2+2(u')^4+6(u')^3+3(u'w')^2\right.$$
$$+4u'(w')^3+(w')^4]+2E_{\bar r\bar\theta}\left[4\left(\frac{u}{\bar r}\right)u'+2\left(\frac{u}{\bar r}\right)(w')^2\right.$$
$$\left.\left.+3\left(\frac{u}{\bar r}\right)(u')^2\right]+4E_{\bar\theta\bar\theta}\left(\frac{u}{\bar r}\right)^2\right\}-\left(\frac{z_{i+1}^2-z_i^2}{2}\right)$$
$$\times\left(\frac{E_{\bar r\bar r}}{w_0}\left[3u'+\frac{5}{2}(u')^2+\frac{3}{2}(w')^2\right]w''+\frac{3u}{\bar r^2w_0}(w')E_{\bar\theta\bar\theta}\right)$$
$$+E_{\bar r\bar\theta}\left\{\frac{3u}{w_0\bar r}w''+(2a-3\bar r)w'[1+(a_1-3\bar r)C_1\right.$$
$$\left.+\bar r(2a-3\bar r)C_2]\right\}+\frac{16w_0}{a^4}\left(\frac{z_{i+1}^3-z_i^3}{3}\right)\left[E_{\bar r\bar r}\left(1+\ell n\frac{\bar r}{a}\right)^2\right.$$
$$\left.+E_{\bar\theta\bar\theta}\ell n^2\left(\frac{\bar r}{a}\right)+2E_{\bar r\bar\theta}\ell n\frac{\bar r}{a}\left(1+\ell n\frac{\bar r}{a}\right)\right] \tag{A4}$$

and

$$\Delta_{jk}=\left(\frac{r_{j+1}^2-r_j^2}{2}\right)(\theta_{k+1}-\theta_k)$$

$$\bar r=\bar r_j=\left(\frac{r_{j+1}+r_j}{2}\right),\qquad \bar\theta=\bar\theta_k=\left(\frac{\theta_{k+1}+\theta_k}{2}\right)$$

$$u'=C_1\frac{w_0^2}{a^3}(a-2\bar r)+C_2\frac{w_0^2}{a^4}(2a\bar r-3\bar r^2)$$

$$w'=\frac{4w_0}{a}\left(\frac{\bar r}{a}\right)\ell n\left(\frac{\bar r}{a}\right),\qquad w''=\frac{4w_0}{a^2}\left(\ell n\frac{\bar r}{a}+1\right) \tag{A5}$$

Failure Criteria Equations

The Tsai-Wu[9] and the maximum stress[7] failure criteria were used in the analysis. Relevant equations for these criteria are given below.

Tsai-Wu Criterion

Failure is assumed to occur when

$$F_{11}\sigma_\ell^2+2F_{12}\sigma_\ell\sigma_t+F_{22}\sigma_t^2+F_{66}\tau_{\ell t}^2+F_1\sigma_\ell+F_2\sigma_t\geq 1 \tag{A6}$$

where σ_ℓ and σ_t are normal stresses along and across the fiber direction, respectively, and $\tau_{\ell t}$ is the shear stress. The

following strength parameters govern the lamina failure:

$$F_{11} = -\frac{1}{XX'}, \quad F_1 = \frac{1}{X} + \frac{1}{X'}, \quad F_{22} = -\frac{1}{YY'}$$

$$F_2 = \frac{1}{Y} + \frac{1}{Y'}, \quad F_{66} = \frac{1}{S^2}, \quad F_{12} = -\frac{0.5}{\sqrt{XX'YY'}} \tag{A7}$$

where X and X' represent the lamina tensile and compressive strengths in the fiber direction, Y and Y' the strengths perpendicular to the fiber direction, and S the lamina shear strength.

Maximum Stress Criteria

Failure is assumed to occur when any one of the following conditions is satisfied:

$\sigma_l \geq X$, fiber failure

$\sigma_t \geq Y$, transverse tension splitting

$\tau_{lt} \geq S$, shear splitting

and for compressive stresses:

$\sigma_l < X'$, fiber crushing

$\sigma_t < Y'$, matrix crushing (A8)

Acknowledgment

The work of the first author was supported by NASA Grant NAG-1-219.

References

[1] Lee, E. H., "Impact of a Mass Striking a Beam," *Journal of Applied Mechanics*, Vol. 7, Dec. 1940, pp. A129-A138.

[2] Lord Rayleigh, "On the Production of Vibrations by Forces of Relatively Long Duration with the Applications to the Theory of Collisions," *Philosophical Magazine*, Ser. 3, Vol. 11, 1906, p. 283.

[3] Greszczuk, L. B., "Damage in Composite Materials Due to Low Velocity Impact," *Impact Dynamics*, edited by L. A. Zukas et al., John Wiley & Sons, New York, 1982, p. 55.

[4] Bostaph, G. M. and Elber, W., "Static Indentation on Composite Plates for Impact Susceptability Evaluation," Proceedings of the Army Symposium on Solid Mechanics, MS 82-4, Mass., Sept. 1982, p. 58.

[5] Elber, W., "Deformation and Failure Mechanics in Low Velocity Impacts on Thin Composite Laminates," NASA TP 2152, May 1983.

[6] Timoshenko, S. and Woinowsky-Krieger, S., *Theory of Plates and Shells*, McGraw-Hill Book Co., New York, 1959.

[7] Jones, R. M., *Mechanics of Materials*, McGraw-Hill Book Co., New York, 1975.

[8] Reissner, E., "On Finite Deflections of Circular Plates," *Proceedings of the Symposia on Applied Mathematics*, American Mathematical Society, New York, Vol. 1, 1949, p. 213.

[9] Tsai, S. W. and Hahn, H. T., *Introduction to Composite Materials*, Technomic, Westport, Conn., 1980.

[10] Dorey, G., "Relationships Between Impact Resistance and Fracture Toughness in Advanced Composite Materials," *50th Meeting of AGARD Structures and Materials Panel*, Athens, AGARD-CP-288, April 1980, p. 9-1.